Arabian Journal for Science and Engineering (2019) 44:6167–6178
https://doi.org/10.1007/s13369-018-03708-3

RESEARCH ARTICLE - PETROLEUM ENGINEERING

Effect of Silica Nanofluid on Nanoscopic Pore Structure of Low-Permeability Petroleum Reservoir by Nitrogen Adsorption Technique: A Case Study

Caspar Daniel Adenutsi[1,2] · Zhiping Li[1,2] · Zhichao Xu[3] · Anthony Edem Hama[4] · Lili Sun[1,5] · Fengpeng Lai[1,2]

Received: 18 July 2018 / Accepted: 24 December 2018 / Published online: 4 January 2019

Abstract
Silica nanofluids have proven to be successful in improving hydrocarbon recovery in the petroleum industry, and increased demand for hydrocarbons has necessitated its application in low-permeability reservoirs. In recent times, surface coating of nanoparticles has been employed to reduce its retention in porous media, but this does not entirely eliminate nanoparticle attachment to pore walls. Knowledge of changes that occur in pore wall and structure such as specific surface area (SSA), pore size distribution and total pore volume (TPV) would be useful in understanding retention mechanisms. This study used nitrogen adsorption technique in studying changes in pore structure due to silica nanofluid treatment. The Brunauer–Emmett–Teller theory and Barrett–Joyner–Halenda adsorption model were used in determining SSAs and TPVs, respectively. SSA, adsorbability and TPV increased in treated samples compared to untreated samples and the rates of change increased with treatment time due to extra pores induced by nanoparticle coagulation. Percent changes in TPV matched closely with SSA and was responsible for increments in the latter. Scanning electron micrographs confirmed coagulation of nanoparticles which increased with treatment time and introduced pseudo-pores on pore walls, resulting in increase in TPV. Increase in differential pore volume was observed for the entire studied range of 2–100 nm except for 3–4 nm which showed no changes in all samples. Severity of differential pore volume increased with treatment time. This study provides insights into nanoscopic changes that occur on pore walls and structure when employing silica nanoparticles in improving hydrocarbon recovery in low-permeability hydrocarbon reservoirs.

Keywords Nitrogen adsorption · Specific surface area · Pore volume · Pore size distribution · Isotherms

1 Introduction

The demand for petroleum and natural gas has necessitated exploration and production of hydrocarbons in low-permeability reservoirs. However, primary recovery of the original hydrocarbon in place is usually very low and secondary recovery performance is dependent on the wettability of the rock matrix [1]. In order to improve hydrocarbon recovery in low-permeability reservoirs, silica nanoparticles have been used to prepare nanofluids that have been employed

✉ Caspar Daniel Adenutsi
casdanad@hotmail.com

Zhiping Li
2002011671@cugb.edu.cn

Zhichao Xu
xuzhichaojerry@163.com

Anthony Edem Hama
aehama.coe@knust.edu.gh

Lili Sun
sunlili0631@163.com

Fengpeng Lai
laifengpeng@cugb.edu.cn

1 School of Energy Resources, China University of Geosciences, Beijing 100083, People's Republic of China

2 Beijing Key Laboratory of Unconventional Natural Gas Geological Evaluation and Development Engineering, Beijing 100083, People's Republic of China

3 National Research Center for Geoanalysis, Beijing 100037, People's Republic of China

4 Rock and Core Properties Laboratory, Department of Petroleum Engineering, Kwame Nkrumah University of Science and Technology, PMB, Kumasi, Ghana

5 Research Institute of Petroleum Exploration and Development, Beijing 100083, People's Republic of China

as an enhanced hydrocarbon recovery agent and found to increase hydrocarbon production [1–5].

A hydrophilic silica nanoparticle with primary size of 7 nm was employed by Hendraningrat et al. [3] in Berea sandstones of permeabilities ranging from 5 to 20 mD. A series of core flooding experiments confirmed increased oil recovery in the low-permeability reservoirs with an optimized nanofluid concentration of 0.05 wt% having a displacement efficiency of 25%. Other similar studies were carried out on low- to medium-permeability (9–35 mD) sandstone using silica nanofluid, and increased oil production was reported after core flooding [4,6]. In another study, the effects of some parameters influencing oil recovery process due to silica nanoparticles such as particle size, rock permeability, initial rock wettability, injection rate and temperature were investigated [5]. Lu et al. [1] performed eleven core flooding tests on sandstone cores with permeabilities less than 1 mD using silica nanoparticles and reported that oil production improved by 4.48–10.33%. Meanwhile, by measuring the composition of effluent fluids it was shown that silica nanoparticles were retained in the porous media. The main mechanisms for improved recovery using silica nanoparticles include wettability alteration, increase in structural disjoining pressure and reduction in interfacial tension [7–14]. Although silica nanoparticles have been reported to increase oil recovery, concerns have been raised about its propagation through porous media as well as its retention on pore walls [11,12,15].

The adverse effect of silica nanoparticles on reservoir properties such as porosity and permeability is as a result of pore throat blockage. Ju et al. [16] developed a simulator that was successfully applied in several oil fields to predict adsorption in pore bodies and blocking of pore throats in sandstone reservoirs by polysilicon nanoparticles and observed reductions in permeability. Previous studies in low-permeability reservoirs suggested that silica nanoparticles have the tendency to block pore network as well as impair porosity and permeability [1,4,6]. Ju and Fan [17] developed a mathematical model to investigate changes in porosity and permeability caused by nanoparticle adsorption and observed declines in instantaneous porosity and permeability. Similar observations were made in medium- to high-permeability reservoirs. Hendraningrat et al. [18] studied the effect of hydrophilic silica nanoparticle on porosity and permeability of high-permeability Berea sandstones and reported 5–88% and 1–11% reductions in liquid permeability and porosity, respectively. To reduce nanoparticle retention in porous media, polymer-coated nanoparticles (PNPs) have been designed and one of the most common polymers used for such purpose is polyethylene glycol (PEG) [15,19]. Some PNPs have surface charge that matches that of the rock reduced adsorption [20–22] but could not eliminate retention in porous media.

Attempts to improve nanoparticle propagation in porous media only reduced retention and adsorption. It is therefore important to understand the changes that occur in pore structure and properties. This study investigates nanoscopic changes that occur with time as a result of silica nanoparticle adsorption on pore walls and structure by nitrogen adsorption technique. Specifically, the effect of nanoparticle on specific surface area (SSA), pore size distributions (PSDs) and pore volume was investigated by comparing the changes that occur in these properties before and after nanofluid treatment. Scanning electron microscopy (SEM) was also utilized to visualize pore walls to corroborate trends and changes in these nanoscopic properties.

2 Materials and Methods

2.1 Core Sample Composition, Preparation and Experimental Fluids

2.1.1 Petrophysical Properties and Mineralogical Composition of Core Sample

In this study, core samples from a typical low-permeability sandstone reservoir were used. The porosity and permeability were measured by KS-VI steady-state porosimeter and permeameter equipment (Jiangsu Hongbo Machinery Manufacturing Co. Ltd, China). The average porosity and permeability of core samples were 13.7% and 10.2 mD, respectively. Parts of the core samples were chipped off and prepared for SEM experiments after which the rest were crushed into various particle size ranges for the purposes of nitrogen adsorption and X-ray diffraction (XRD) experiments.

For purposes of investigating the mineralogical composition of low sandstone sample, part of the core sample was crushed to 320 mesh. XRD was performed using SmartLab-9 X-ray diffractometer (Rigaku Corporation, Japan) with CuKα radiation at 40 kV, 200 mA and a fixed graphite monochromator. The XRD patterns were collected in the 2-theta range of 3°–70° with a scanning rate of 10°/min at room temperature. The XRD pattern is presented in Fig. 1.

The analyzed XRD data (Table 1) showed that the most abundant mineral in the sandstone is the plagioclase feldspar, albite with 64% mineralogical composition, while quartz was second with about 24%. Clay mineralogy of the sandstone sample was chlorite which made up 10% while other accessory minerals included the coarse mica, muscovite, and calcite.

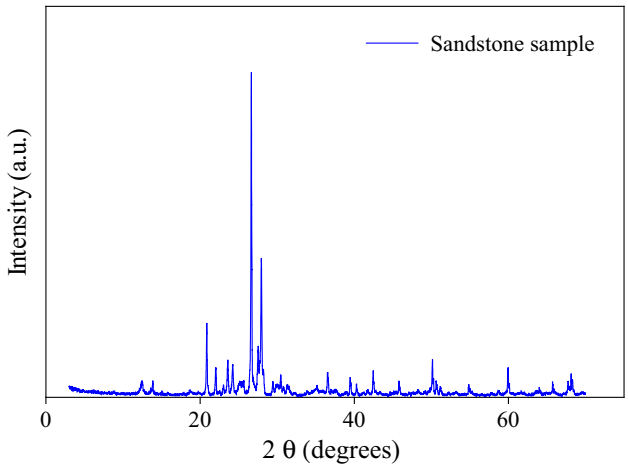

Fig. 1 XRD results of low-permeability sandstone sample

Table 1 Mineral composition of the sandstone sample

Mineral	Quartz	Albite	Calcite	Chlorite	Muscovite
Percentage	24	64	1	10	1

2.1.2 Sample Preparation for Adsorption Experiments and Experimental Fluid

Some of the crushed sample was sieved with a mesh of particle range of 20–60 for the purposes of nitrogen adsorption experiments. The sieved sample was then separated into 4 parts.

A hydrophilic nanoparticle powder (Zhengzhou Dongyao Nano Materials Co. Ltd., China) with single particle size of 7 nm, which consists of 99.9% silicon dioxide (SiO_2), was used in this study (Fig. 2a). Nanofluid with weight concentration of 0.05 wt% was dispersed, first by using a powerful high-speed mechanical stirrer and later with a sonicator for 90 min (Fig. 2b). The nanofluid was used in sample treatment.

2.2 Damage Reactor Design and Operational Procedure for Nanofluid Treatment of Samples

2.2.1 Damage Reactor Design

A special damage reactor was designed for this experiment [23]. For the sake of clarity, the schematic of the reactor is shown in Fig. 3, at atmospheric pressure and at a high pressure.

The reactor consisted of a sample chamber and an outer lid. The outer lid had an inner lid with a rubber ring that ensures an air tight fit into the sample chamber. A pipe with a valve connected to a vacuuming pump passed through the lid into the container. A nanofluid inlet unit consisted of an inlet pipe, and its valve was connected to a pump that ensured complete filling of the reactor at atmospheric conditions. A hydraulic pressure unit was made up of a hydraulic pump, buffer tank, pressure loading valve and a pressure release valve. The bottom of the sample chamber was separated from the hydraulic unit by a movable plate. The hydraulic pump aided in applying a predetermined pressure.

2.2.2 Nanofluid Sample Treatment Procedure

The crushed sample was put into the reactor container and the lid tightly fixed. The sample was then vacuumed for 4 h with all valves closed except the vacuum valve. The vacuum valve was closed afterward, and the nanofluid valve was opened to introduce nanofluid through nanofluid inlet pipe. Next, the nanofluid valve was closed to prevent back flow. By means of a hydraulic pump and with the pressure loading valve opened with the release valve closed, 20 MPa pressure was applied. After 1 h, the pressure release valve was opened and sample particles were taken out, dried and sieved. This procedure was repeated for different treatment times of 3 h, 6 h and 12 h

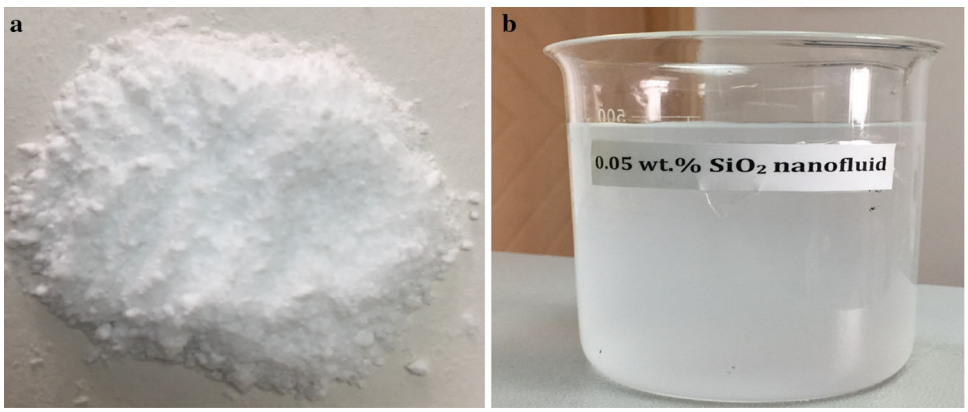

Fig. 2 **a** SiO_2 nanoparticles, **b** 0.05 wt% SiO_2 nanofluid

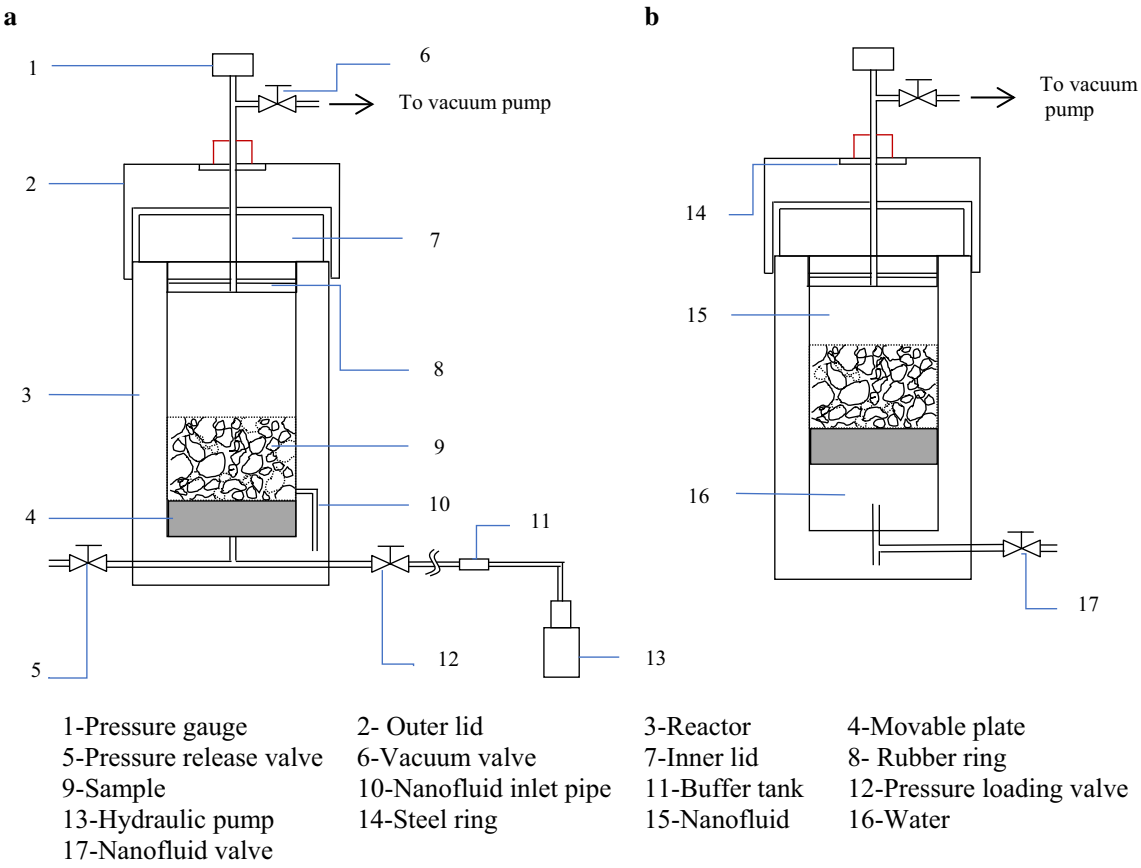

Fig. 3 Schematic diagram of core damage reactor at **a** atmospheric pressure, **b** high pressure

2.3 N_2 Adsorption–Desorption Measurements

N_2 adsorption–desorption experiments were carried out with 3H-2000PS2 SSA and porosity analyzer produced by Beesd Instrument Technology (Beijing) Co., Ltd (Fig. 4a).

The static volumetric method was employed in representing effect of nanoparticle on reservoir pore structure. Four samples were labeled 1 h, 3 h, 6 h and 12 h for adsorption experiments. N_2 adsorption–desorption isotherms were measured at relative pressures ranging from 0.01 to 0.995 at 77 K. N_2 adsorption–desorption test was then repeated for all the samples after nanofluid treatment to investigate the effect of nanoparticle adsorption time on reservoir pore structure. The static volumetric method is described as follows: The crushed sample was weighed and vacuumed at 200 °C for 12 h to remove any residual air which was adsorbed on the surface of particles. The sample which was put in its holder was fixed in the adsorption manifold. The sample holder was kept at liquid nitrogen temperature (77 K). The saturated vapor pressure of N_2 (P_0) at the experimental temperature was measured. Consecutive known amounts of N_2 was introduced by means of injection into the sample holder. After equilibrium pressure (P) had been established due to adsorption of the gas onto the samples, the pressure and the amount of gas adsorbed were recorded. The injection system was made up of a calibrated piston, which automatically varied both the pressure and the injected volume. A series of pressure test points were preset. These points ranged from 0 to P_0. The experiment was started at a high vacuum, and step by step, the pressure was automatically increased close to the nitrogen saturation pressure. For each known volume of adsorbed gas (V), a relative pressure ($P/P_{0)}$ was computed. The adsorption branch of the isotherm was constructed by plotting relative pressure (on the abscissa) versus the amount of nitrogen adsorbed (on the ordinate). Similarly, the desorption branch of the isotherm was constructed by gradually reducing the pressure in a stepwise manner.

2.4 Scanning Electron Microscopy Experiments

Pore morphology and adsorption of nanoparticles onto pore walls were visualized by the aid of Zeiss Supra 55 Sapphire scanning electron microscope (Fig. 4b). Parts of the core sample were chipped off and five stubs of approximate dimensions 10 mm × 5 mm × 5 mm were prepared. Four of these stubs were treated with nanofluid for 1 h, 3 h, 6 h and

Fig. 4 **a** Nitrogen adsorption equipment, **b** scanning electron microscope

12 h in the reactor as described in Sect. 2.2.2. The last sample was left untreated. All five stubs were dried and coated with thin platinum film. Multiple point photographs were taken at 50 K and 200 K times magnifications and statistically frequent characteristics picked out as general results.

2.5 Analytical Methods

The Brunauer–Emmett–Teller (BET) theory was applied to evaluate specific surface area (SSA) [24]. This is by far the most appropriate approach of determining SSA [25]. The classical BET equation is given by:

$$\frac{1}{V\left[(P_0/P)-1\right]} = \frac{1}{V_m C} + \frac{C-1}{V_m C}\left(\frac{P}{P_0}\right) \tag{1}$$

A plot of $1/V\left[(P_0/P)-1\right]$ versus P/P_0 gives a straight line in the range $0.05 \leq P/P_0 \leq 0.35$. In this range of P/P_0, parameters V_m and C can be evaluated by Eq. (1) and deemed as accurate provided the volumes of adsorbed gas measured from experiments are higher than V_m calculated from the BET equation [26,27]. All volumes of adsorbed gas measured from experiments which were less than V_m were considered unreasonable and were ignored. From the intercept and slope derived from Eq. (1), V_m and C can be evaluated as $1/(s+i)$ and $(s/i)+1$, respectively. The adsorbance can then be evaluated at any P/P_0 after unreasonable data points are ignored [28]. The adsorbance at $P/P_0 = 0.35$ was evaluated by Eq. (2):

$$V_{P/P_0} = V_m \frac{C\frac{P}{P_0}}{\left(1-\frac{P}{P_0}\right)\left[1+(C-1)\frac{P}{P_0}\right]} \tag{2}$$

In Eqs. (1) and (2), V is volume of adsorbed gas measured from experiment at a particular relative pressure, mL/g; V_m is the volume of mono-molecular layer of gas, mL/g; V_{P/P_0} is volume of gas at $P/P_0 = 0.35$, mL/g; C is the BET constant, P is the equilibrium adsorption pressure of N_2 at the experimental temperature (77 K), bar; P_0 is the saturated vapor pressure of N_2 at the experimental temperature (77 K), bar; P/P_0 is relative pressure, fraction; and s and i are slope and intercept graphically evaluated from the BET equation, respectively.

In this investigation, the pore size distribution and total pore volumes were evaluated based on the adsorption branch isotherm with the Barrett–Joyner–Halenda (BJH) model [29]. This is because the tensile strength effect contributes extra pores based on desorption isotherms [30].

The details of the analytical models and theories employed in this investigation are comprehensively discussed in the literature [24,25,27,29,31,32].

3 Results and Discussion

3.1 Qualitative Description of Pore Morphology from Adsorption Isotherms

Isotherms of samples showed similar characteristics (Fig. 6). According to the International Union of Pure and Applied Chemistry (IUPAC) nomenclature, the shape of the N_2 adsorption–desorption isotherms indicates Type II isotherm (see Fig. 5a) with H3 hysteresis loop (see Fig. 5b) [25,33]. However, some studies considered this type of isotherm as Type IV (see Fig. 5a) due to the presence of hysteresis loop [34,35]. Although the primary characteristic feature of Type IV isotherms is a hysteresis loop due to capillary condensation, another typical feature is a final saturation plateau over a range of high P/P_0, indicating complete pore filling (see Fig. 5a) [25,36]. The isotherms from this investigation lacked saturation plateau at high P/P_0. Xu et al. [26] explained with evidence that this behavior is due to the presence of some macropores and suggested these types of isotherms are

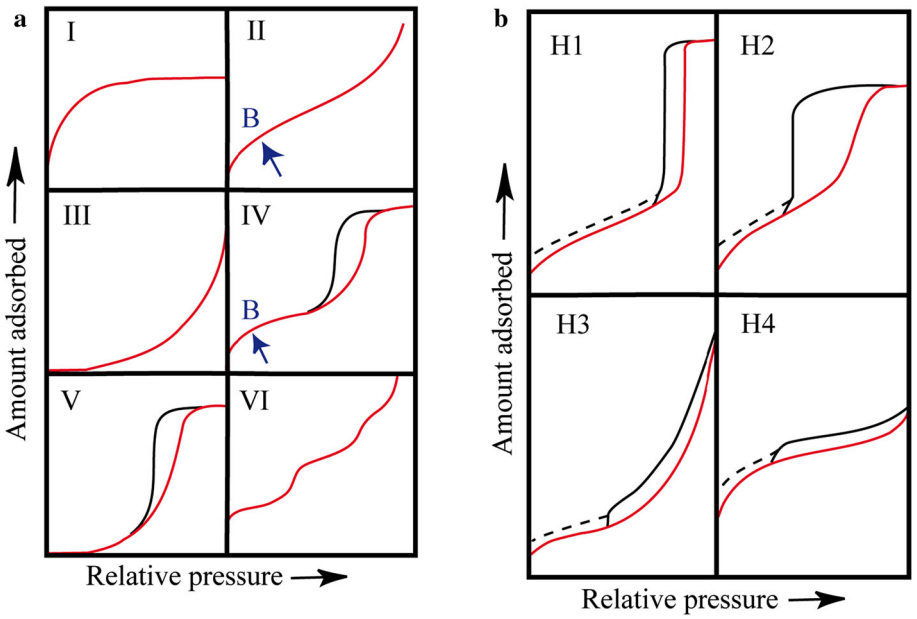

Fig. 5 IUPAC classifications of **a** isotherms, **b** hysteresis loops; modified according to [27]

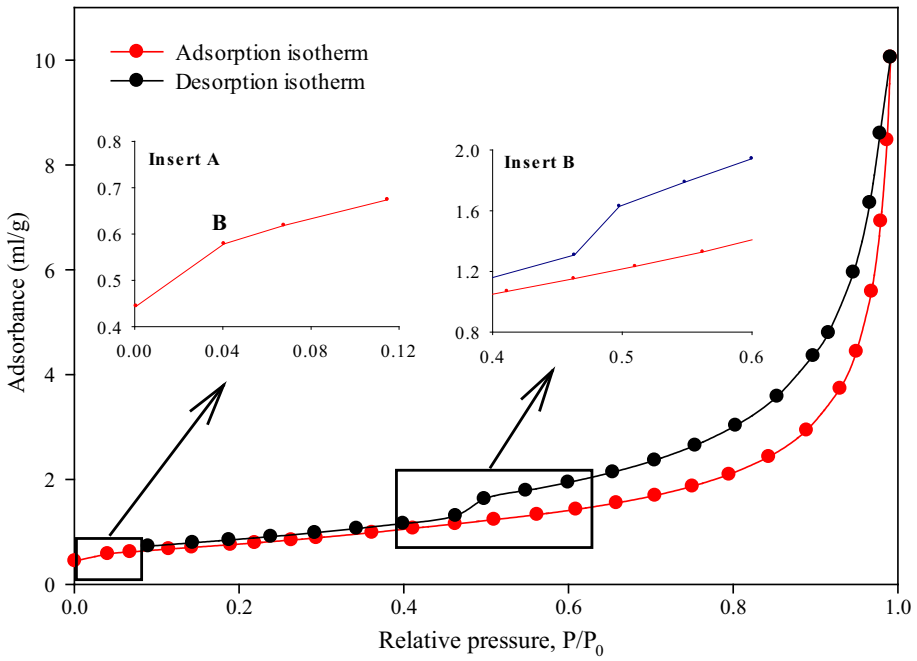

Fig. 6 Isotherm of sample showing inflection point and H3 hysteresis loop

primarily Type II associated with unrestricted monolayer–multilayer adsorption of macroporous adsorbents.

One of the features of the isotherms was the presence of knee or inflection point (B) at low P/P_0 (Fig 6, insert A). This indicated the stage at which monolayer adsorption was complete and the beginning of multilayer adsorption process. Moreover, adsorbance sharply increased and the curves showed hysteresis loop over a range of moderate to high P/P_0 due to capillary condensation. This was indicative of the presence of mesopores in samples. Furthermore, adsorbance increased without saturation plateau over a range of high P/P_0, indicating a probable presence of macropores. Ultimately, according to IUPAC the H3 hysteresis loop is often attributed to non-rigid aggregates of plate-like particles with macroporous pore network which is indicative of slit-shaped pores [25,33]. Inferring from the shape of the isotherms, it was deduced that the samples contained slit-shaped mesopores and some macropores.

3.2 Changes in Isotherms Due to Nanofluid

Obvious changes which varied with nanofluid treatment time were displayed in isotherms of treated samples (Fig. 7).

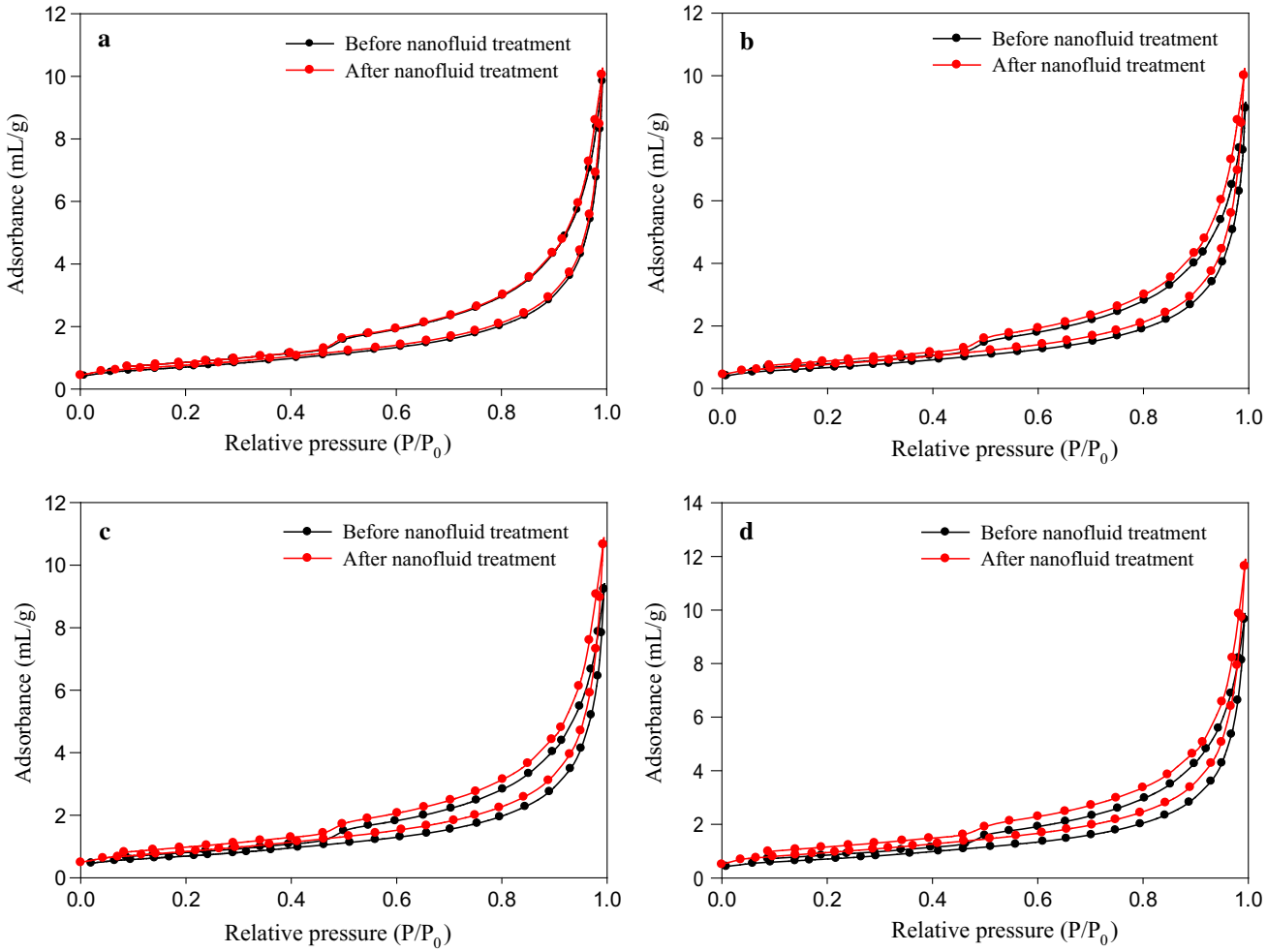

Fig. 7 Effect of silica nanofluid on isotherms for different treatment times: **a** 1 h, **b** 3 h, **c** 6 h, **d** 12 h

Noticeable in this study was upward shifts in hysteresis loops of samples treated with nanofluid, and the severity of the shift increased with time. Negligible upward shift was observed for the sample treated for 1 h, while samples treated for 3, 6 and 12 h exhibited more severe changes. The changes could be attributed to nanoparticle deposition and adsorption on pore walls which probably changed the original pore wall composition and structure. Adsorption of nanoparticles on pore walls increased with time (Fig. 7), causing severe upward shift in samples treated for longer time periods.

Secondly, maximum adsorbance increased in treated samples compared to untreated samples and the rates of change increased with treatment time (Table 2). The increase in maximum adsorbance could be due to deposition of nanoparticles on pore surfaces. These nanoparticles coagulated introducing intergranular pores in the sample system which would be detected as extra pores by N_2 gas molecules, thereby increasing adsorbance. Coagulation increased with increase in treatment time introducing more pores which could cause the observed percentage increase in maximum adsorbance with time.

Table 2 Effect of nanofluid on maximum adsorbance

Sample	1 h	3 h	6 h	12 h
Before (mL/g)	9.8485	8.9635	9.2306	9.6591
After (mL/g)	10.0512	10.012	10.6617	11.639
Change (%)	2.06	11.70	15.50	20.50

3.3 Changes in Pore Wall Properties Based on BET Theory

3.3.1 Effect of Nanofluid on BET SSA

Table 3 presents SSA of treated and untreated samples. It was observed that there was a general increase in SSA of damaged samples as compared to undamaged samples. The increment in SSA could be due to detection of smaller pores

Table 3 Effect of silica nanofluid on BET SSA

Sample (h)	SSA before damage (m^2/g)	SSA after damage (m^2/g)	Change in SSA (%)
1	2.5763	2.7673	7.41
3	2.4188	2.7797	14.92
6	2.518	3.0458	20.96
12	2.5902	3.4226	32.14

by N_2 molecules. Coagulation of nanoparticles on pore walls could introduce more pores which would be detected as extra smaller pores, increasing the SSA of samples. Also, increase in surface roughness of pore walls due to nanoparticle adsorption which could also be partly responsible for the observed increase. SEM micrographs confirmed surface roughness of samples treated with nanoparticles (Figs. 10b, 11a–d), and this is further discussed in Sect. 3.5.

The study revealed that the percentage change in SSA in treated samples increased with treatment time which implied smaller pores increased with time due to coagulation. Furthermore, surface roughness of pore walls could also increase as more nanoparticles got attached to pores surfaces. Although nanoparticle coagulation could block some original smaller pores of samples, the amount of nanoparticle deposition and coagulation increased with time taking precedence over pore blockage. SEM micrographs of samples corroborated increase in coagulation with treatment time (Fig. 11a–d). This phenomenon would increase smaller intergranular pores within the system and perhaps render pore surfaces rougher accounting for the observation.

3.3.2 Effect of Nanofluid on Adsorbability

Notably, the adsorbance of monolayer as well as multilayers increased in treated samples compared to untreated samples and the rates of changes increased with treatment time (Table 4). However, increment in multilayer adsorption was slightly higher than that of monolayers. Contribution to adsorbance of multilayers was thus determined as the differences between percent changes in monolayer and multilayer adsorbances. Multilayer contribution ranged between 0.07 and 1.49% (Table 4). Percent increases in adsorption and BET SSA matched closely. This meant that coagulation of nanoparticles caused increments in adsorbability and probably accounted for changes in SSA.

3.4 Changes in Pore Structure Based on BJH Model

3.4.1 Effect of Nanofluid on PSD

Pore size distributions (PSDs) of all treated and untreated samples displayed unimodal peaks between 2 and 3 nm, suggesting that most of studied pores were mesopores. This accounted for the hysteresis loop displayed in isotherms in Sects. 3.1 and 3.2.

Noticeably, samples treated with nanofluid displayed obvious variations compared with untreated samples (Fig. 8). These changes varied with treatment time and gave insight into changes that occurred with nanoparticle deposition and retention. Firstly, minimal changes occurred in the sample treated for 1 h and there was slight increase in differential pore volume of meso-macro pores between 20–80 nm. However with increase in treatment time, there was an increase in differential pore volume within mesopore range of 2–3 nm and meso-macro pore range of 5–80 nm, and these variations increased with time (Fig. 8b–d). Although there was a general increase in differential pore volume, there was blockage effect of mesopores by nanoparticles within 3–4 nm range in all samples.

The results implied that after nanoparticle treatment extra pores were detected by N_2. This could be attributed to coagulation of nanoparticles which induced extra intergranular pore in the network. This observation accounted for the increased maximum adsorption and an upward shift in isotherms for treated samples displayed in Sect. 3.2. Moreover, the changes suggested that nanoparticle invasion and deposition initially started in meso-macro pores (Fig. 8a). With increase in treatment time, nanoparticles invaded smaller mesopores and coagulation increased, thereby inducing more pores (Fig. 8b–d). The blockage effect observed in 3–4 nm range suggested that there was blockage of pores and pore throats in this diameter range.

Table 4 Changes in adsorption of first and multilayers

Samples (h)	Monolayer adsorption (V_m)			Multilayer adsorption ($V_{0.35}$)			Multilayer contribution (%)
	Before treatment (mL/g) (mL/g)	After treatment (mL/g)	Change (%)	Before treatment (mL/g)	After treatment (mL/g)	Change (%)	
1	0.5992	0.6396	6.74	0.8962	0.9664	7.83	1.09
3	0.5565	0.6388	14.80	0.8411	0.9662	14.87	0.07
6	0.5796	0.7033	21.35	0.8733	1.0613	21.52	0.17
12	0.6004	0.7864	30.98	0.8990	1.1909	32.47	1.49

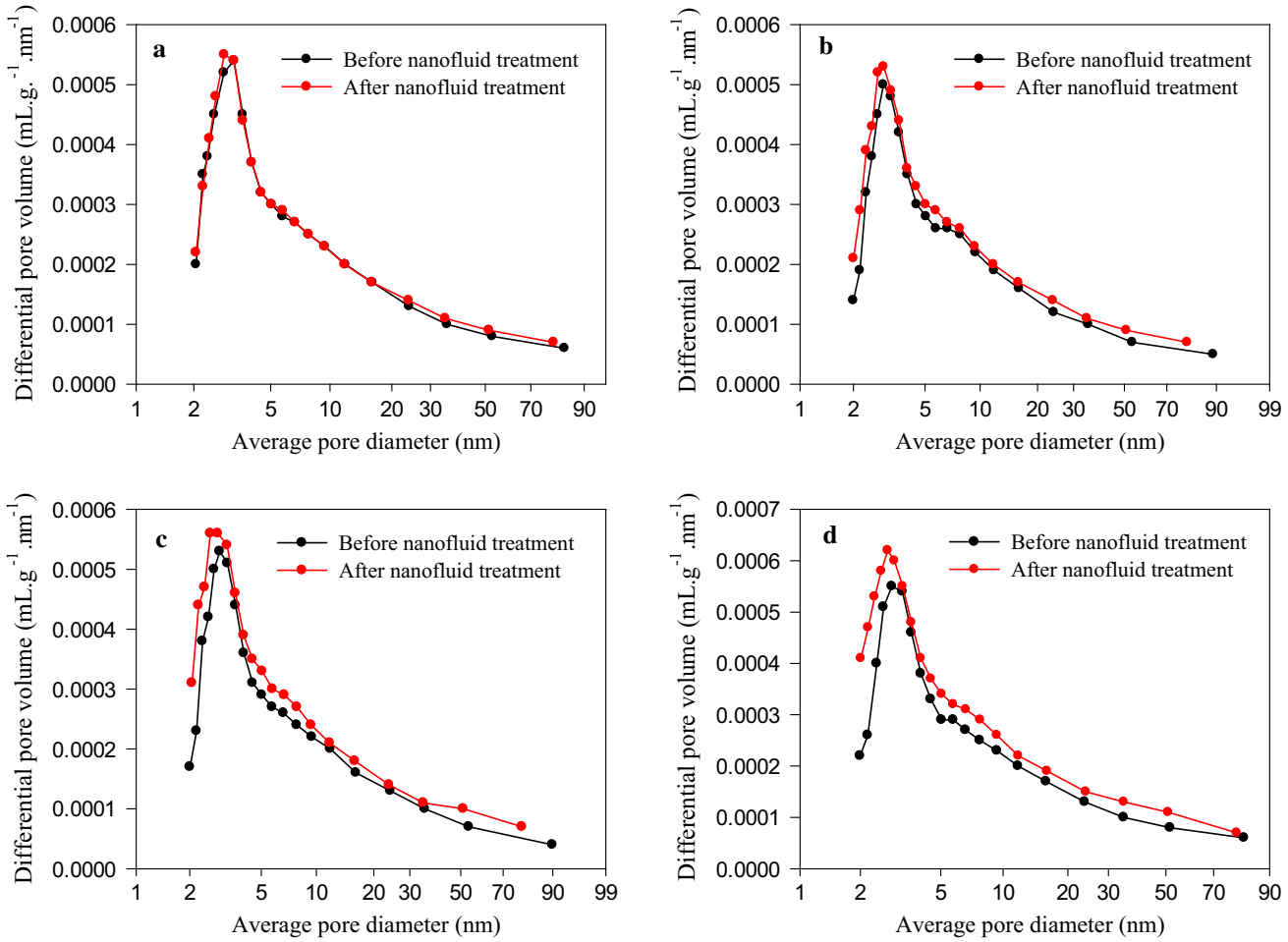

Fig. 8 Effect of silica nanofluid on PSD for different treatment times: **a** 1 h, **b** 2 h, **c** 6 h, **d** 12 h

Table 5 Effect of silica nanofluid on pore volume range of 2–100 nm

Sample (h)	Mesopore pore volume			Macropore pore volume			Total pore volume		
	Before treatment (μL/g)	After treatment (μL/g)	% Change	Before treatment (μL/g)	After treatment (μL/g)	% Change	Before treatment (μL/g)	After treatment (μL/g)	% Change
1	8.28	8.52	2.90	3.36	3.67	9.23	11.64	12.19	4.73
3	7.67	8.2	6.91	2.83	4.06	43.46	10.49	12.26	16.87
6	7.92	9.05	14.27	2.76	3.83	38.77	10.68	12.89	20.69
12	8.31	9.85	18.53	2.29	3.85	68.12	10.6	13.7	29.24

3.4.2 Effect of Nanofluid on Pore Volume

It was revealed in this study that mesopore, macropore and total pore volumes increased in samples treated with nanofluid compared to untreated samples, based on studied pores.

Furthermore, percent change in total pore volume increased with increasing time. This implied invasion and coagulation increased with time, thereby inducing more pores which contributed to pore volume. Although there were slight differences, the ranges of percent increment in total pore volume in damaged samples were in accordance with BET SSA percent increments (compare Tables 3, 5). It could be deduced that the increment in total pore volume as a result of invasion and coagulation was the paramount reason for increment in SSAs and adsorbability.

Although this study observed increase in pore volume due to nanoparticle coagulation, these nanoparticles actually coagulated on pore walls and in pore throats. Section 3.5

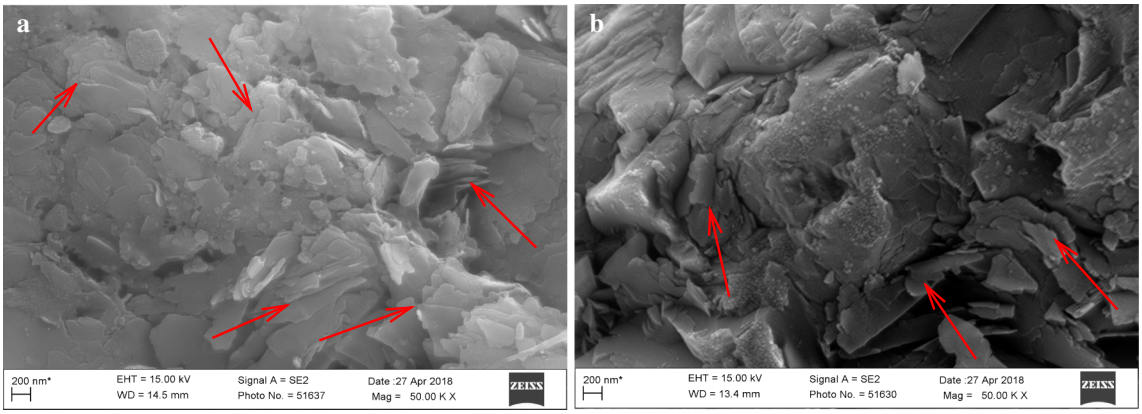

Fig. 9 Plate-like particles 50 K times magnification, **a** 1 h, **b** 6 h

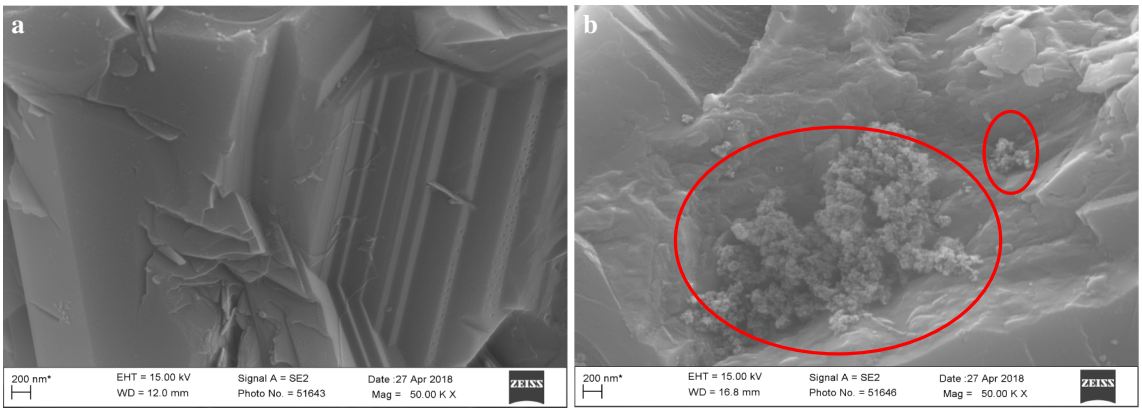

Fig. 10 SEM Micrographs at 50 K times magnification, **a** untreated sample, **b** treated sample 12 h

provided visual evidence by means of SEM micrographs as a support to this claim.

3.5 Effect of Silica Nanofluid on Pore Morphology by SEM

The surface morphology of samples was studied using SEM to show changes in structure of pore surfaces and also enhance understanding of changes in adsorption isotherms, adsorbability, SSA, PSD and total pore volumes.

Samples showed aggregates of plate-like particles (Fig. 9). Plate-like aggregates display H3 hysteresis loop [25,27], and this was observed in Sect. 3.1 and thus served as supporting evidence to the claim of slit-shaped pores of samples.

Comparing untreated to treated samples, it was observed that the surfaces of treated samples were rougher (compare Fig. 10a, b. Compare Figs. 10a, 11a–d). This may be partly responsible for increase in SSAs. Also, it was observed that, nanoparticles coagulated on pore walls and throats (Fig. 10b). The attachment and coagulation was responsible for changes in adsorption isotherms as composition of pore walls changed. Coagulation introduced extra pores, and this explained why SSA, adsorbability, PSD and pore volume increased in treated samples compared to untreated samples. The increase in these properties was due to the induced intergranular pores which were detected by N_2 molecules. The affinity for water coupled with the presence of these extra pores could be responsible for increases in initial water saturation observed in a previous study when hydrophilic nanoparticles were employed during core flooding experiment [1] as water could be held in them due to capillary forces. However, it was observed that nanoparticles were retained in some pore throats (Fig 10b).

The study revealed that nanoparticle coagulation increased with time (Fig. 11a–d). This meant extra pores increased with treatment time. This explained why SSA, adsorbability and total pore volume increased with treatment time.

4 Conclusions

Changes in nanoscopic pore structure, BET SSA, adsorbability, PSDs and total pore volume were studied by N_2 adsorption technique. SEM was employed for nanoscopic visualization of changes on pore walls, and the following conclusions could be drawn:

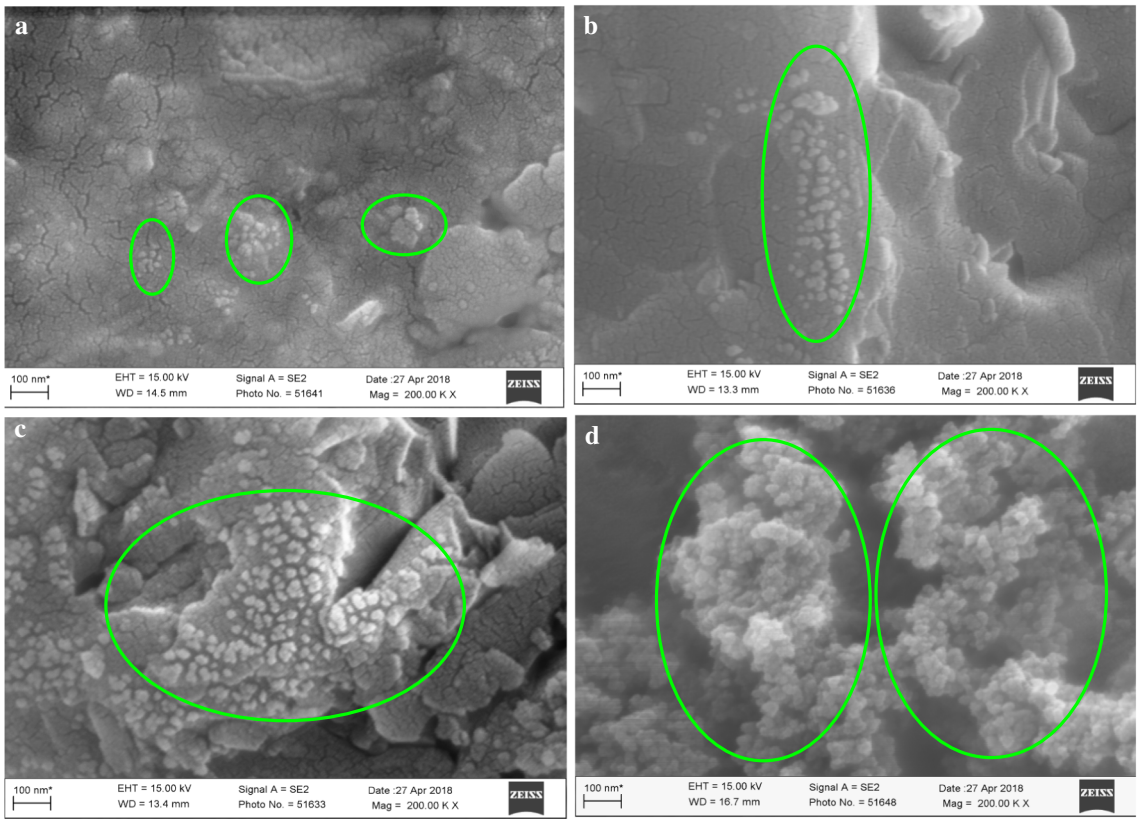

Fig. 11 SEM micrographs showing nanoparticle coagulation at 200 K times magnification, **a** 1 h, **b** 3 h, **c** 6 h, **d** 12 h

1. Type II isotherms with H3 hysteresis loop were displayed in both treated and untreated samples. SEM micrographs confirmed plate-like particles associated with H3 hysteresis loop.
2. SSA and total pore volume (TPV) increased in treated samples compared to untreated samples. The percent increase in these parameters of treated samples increased with treatment time.
3. Increase in differential pore volume was observed for the entire studied range of 2–100 nm except for 3–4 nm which showed no changes in all samples. Severity of differential pore volume increased with treatment time.
4. Percent increments in total pore volume matched closely with that of SSA. Increments in total pore volume and roughness of pore walls due to nanoparticle deposition are responsible for SSA increments.
5. Coagulation of nanoparticles which increased with treatment time introduced pseudo-pores in treated samples which were the main factor that caused nanoscopic changes in pore structure.

Acknowledgements The authors would like to express their profound gratitude to Dr. Philip Antwi and Dr. Samuel Barnie for their help in the preparation of this manuscript. This research was supported by the National Science and Technology Major Project of China (Grant No. 2017ZX05009-005).

References

1. Lu, T.; Li, Z.; Zhou, Y.; Zhang, C.: Enhanced oil recovery of low-permeability cores by SiO_2 nanofluid. Energy Fuels **31**(5), 5612–5621 (2017)
2. Wang, K.L.; Liang, S.C.; Wang, C.C.: Research of improving water injection effect by using active SiO_2 nano-powder in the low-permeability oilfield. Adv. Mater. Res. **92**, 207–212 (2010)
3. Hendraningrat, L.; Li, S.; Torsaeter, O.: Enhancing oil recovery of low-permeability Berea sandstone through optimised nanofluids concentration. In: SPE Enhanced Oil Recovery Conference. Society of Petroleum Engineers (2013)
4. Hendraningrat, L.; Li, S.; Torsæter, O.: A coreflood investigation of nanofluid enhanced oil recovery. J. Petrol. Sci. Eng. **111**, 128–138 (2013)
5. Hendraningrat, L.; Li, S.; Torsater, O.: Effect of some parameters influencing enhanced oil recovery process using silica nanoparticles: an experimental investigation. In: SPE Reservoir Characterization and Simulation Conference and Exhibition. Society of Petroleum Engineers (2013)
6. Hendraningrat, L.; Li, S.; Torsater, O.: A coreflood investigation of nanofluid enhanced oil recovery in low-medium permeability Berea sandstone. In: SPE International Symposium on Oilfield Chemistry. Society of Petroleum Engineers (2013)
7. Wasan, D.T.; Nikolov, A.D.: Spreading of nanofluids on solids. Nature **423**(6936), 156 (2003)
8. Roustaei, A.; Moghadasi, J.; Bagherzadeh, H.; Shahrabadi, A.: An experimental investigation of polysilicon nanoparticles' recovery efficiencies through changes in interfacial tension and wettability alteration. In: SPE International Oilfield Nanotechnology Conference and Exhibition. Society of Petroleum Engineers (2012)

9. Cheraghian, G.: Effects of nanoparticles on wettability: a review on applications of nanotechnology in the enhanced oil recovery. Int. J. Nano Dimens. **6**(5), 443 (2015)
10. Cheraghian, G.; Hendraningrat, L.: A review on applications of nanotechnology in the enhanced oil recovery Part A: effects of nanoparticles on interfacial tension. Int. Nano Lett. **6**(2), 129–138 (2016)
11. Cheraghian, G.; Hendraningrat, L.: A review on applications of nanotechnology in the enhanced oil recovery Part B: effects of nanoparticles on flooding. Int. Nano Lett. **6**(1), 1–10 (2016)
12. Sun, X.; Zhang, Y.; Chen, G.; Gai, Z.: Application of nanoparticles in enhanced oil recovery: a critical review of recent progress. Energies **10**(3), 345 (2017)
13. Ju, B.; Fan, T.; Li, Z.: Improving water injectivity and enhancing oil recovery by wettability control using nanopowders. J. Petrol. Sci. Eng. **86**, 206–216 (2012)
14. Kamal, M.S.; Adewunmi, A.A.; Sultan, A.S.; Al-Hamad, M.F.; Mehmood, U.: Recent advances in nanoparticles enhanced oil recovery: rheology, interfacial tension, oil recovery, and wettability alteration. J. Nanomater. **2017**, 15 (2017)
15. ShamsiJazeyi, H.; Miller, C.A.; Wong, M.S.; Tour, J.M.; Verduzco, R.: Polymer-coated nanoparticles for enhanced oil recovery. J. Appl. Polym. Sci. **131**(15), 1–13 (2014)
16. Ju, B.; Dai, S.; Luan, Z.; Zhu, T.; Su, X.; Qiu, X.: A study of wettability and permeability change caused by adsorption of nanometer structured polysilicon on the surface of porous media. In: SPE Asia Pacific Oil and Gas Conference and Exhibition. Society of Petroleum Engineers (2002)
17. Ju, B.; Fan, T.: Experimental study and mathematical model of nanoparticle transport in porous media. Powder Technol. **192**(2), 195–202 (2009)
18. Hendraningrat, L.; Engeset, B.; Suwarno, S.; Li, S.; Torsæter, O.: Laboratory investigation of porosity and permeability impairment in Berea sandstones due to hydrophilic nanoparticle retention. Paper SCA2013-062 Presented at the International Symposium of the Society of Core Analysts Held in Napa Valley, pp. 16–19, California (2013)
19. Negin, C.; Ali, S.; Xie, Q.: Application of nanotechnology for enhancing oil recovery—a review. Petroleum **2**(4), 324–333 (2016)
20. Yang, G.C.; Tu, H.-C.; Hung, C.-H.: Stability of nanoiron slurries and their transport in the subsurface environment. Sep. Purif. Technol. **58**(1), 166–172 (2007)
21. Bagaria, H.G.; Neilson, B.M.; Worthen, A.J.; Xue, Z.; Yoon, K.Y.; Cheng, V.; Lee, J.H.; Velagala, S.; Huh, C.; Bryant, S.L.: Adsorption of iron oxide nanoclusters stabilized with sulfonated copolymers on silica in concentrated NaCl and CaCl2 brine. J. Colloid Interface Sci. **398**, 217–226 (2013)
22. Kim, H.-J.; Phenrat, T.; Tilton, R.D.; Lowry, G.V.: Effect of kaolinite, silica fines and pH on transport of polymer-modified zero valent iron nano-particles in heterogeneous porous media. J. Colloid Interface Sci. **370**(1), 1–10 (2012)
23. Li, Z.; Xu, Z.: A reactor for core damage by supercritical CO_2 under high temperature and high pressure conditions. Chinese Patent, CN201510484941.1 China (2017)
24. Brunauer, S.; Emmett, P.H.; Teller, E.: Adsorption of gases in multimolecular layers. J. Am. Chem. Soc. **60**(2), 309–319 (1938)
25. Thommes, M.; Kaneko, K.; Neimark, A.V.; Olivier, J.P.; Rodriguez-Reinoso, F.; Rouquerol, J.; Sing, K.S.: Physisorption of gases, with special reference to the evaluation of surface area and pore size distribution (IUPAC technical report). Pure Appl. Chem. **87**(9–10), 1051–1069 (2015)
26. Xu, Z.; Li, Z.; Wang, C.; Adenutsi, C.D.: Experimental study on microscopic formation damage of low permeability reservoir caused by HPG fracturing fluid. J. Nat. Gas Sci. Eng. **36**, 486–495 (2016)
27. Lowell, S.; Shields, J.E.; Thomas, M.A.; Thommes, M.: Characterization of Porous Solids and Powders: Surface Area, Pore Size and Density. Springer, Berlin (2012)
28. Lowell, S.: The BET constant and site occupancy. Powder Technol. **12**(3), 291–293 (1975)
29. Barrett, E.P.; Joyner, L.G.; Halenda, P.P.: The determination of pore volume and area distributions in porous substances. I. Computations from nitrogen isotherms. J. Am. Chem. Soc. **73**(1), 373–380 (1951)
30. Groen, J.C.; Peffer, L.A.; Pérez-Ramırez, J.: Pore size determination in modified micro-and mesoporous materials. Pitfalls and limitations in gas adsorption data analysis. Microporous Mesoporous Mater. **60**(1–3), 1–17 (2003)
31. Kuila, U.; Prasad, M.: Specific surface area and pore-size distribution in clays and shales. Geophys. Prospect. **61**(2), 341–362 (2013)
32. Gregg, S.; Sing, K.: Adsorption, Surface Area and Porosity, 2nd edn, p. 303. Academic, New York (1982)
33. Sing, K.S.: Reporting physisorption data for gas/solid systems with special reference to the determination of surface area and porosity (Recommendations 1984). Pure Appl. Chem. **57**(4), 603–619 (1985)
34. Ramesh, K.; Reddy, K.S.; Rashmi, I.; Biswas, A.: Porosity distribution, surface area, and morphology of synthetic potassium zeolites: a SEM and N2 adsorption study. Commun. Soil Sci. Plant Anal. **45**(16), 2171–2181 (2014)
35. Shao, X.; Pang, X.; Li, Q.; Wang, P.; Chen, D.; Shen, W.; Zhao, Z.: Pore structure and fractal characteristics of organic-rich shales: a case study of the lower Silurian Longmaxi shales in the Sichuan Basin, SW China. Mar. Petrol. Geol. **80**, 192–202 (2017)
36. Clarkson, C.R.; Solano, N.; Bustin, R.M.; Bustin, A.; Chalmers, G.; He, L.; Melnichenko, Y.B.; Radliński, A.; Blach, T.P.: Pore structure characterization of North American shale gas reservoirs using USANS/SANS, gas adsorption, and mercury intrusion. Fuel **103**, 606–616 (2013)